Recent anthropogenic curtailing of Yellow River runoff and sediment load is unprecedented over the past 500 y

Yu Liu[a,b,c,d,1], Huiming Song[a,b,e], Zhisheng An[a,b,e,1], Changfeng Sun[a,b], Valerie Trouet[f], Qiufang Cai[a,b,c], Ruoshi Liu[d], Steven W. Leavitt[f], Yi Song[a], Qiang Li[a,b,e], Congxi Fang[a], Weijian Zhou[a,b], Yinke Yang[g], Zhao Jin[a,b], Yunqiang Wang[a,b], Junyan Sun[a], Xingmin Mu[h], Ying Lei[a], Lu Wang[a], Xuxiang Li[d], Meng Ren[a], Linlin Cui[a], and Xueli Zeng[a]

[a]The State Key Laboratory of Loess and Quaternary Geology, Institute of Earth Environment, Chinese Academy of Sciences, 710061 Xi'an, China; [b]CAS Center for Excellence in Quaternary Science and Global Change, Chinese Academy of Sciences, 710061 Xi'an, China; [c]Open Studio for Oceanic-Continental Climate and Environment Changes, Pilot National Laboratory for Marine Science and Technology, 266061 Qingdao, China; [d]School of Human Settlements and Civil Engineering, Xi'an Jiaotong University, 710049 Xi'an, China; [e]Interdisciplinary Research Center of Earth Science Frontier, Beijing Normal University, 100875 Beijing, China; [f]Laboratory of Tree-Ring Research, The University of Arizona, Tucson, AZ 85721; [g]School of Environmental Science and Engineering, Chang'an University, 710054 Xi'an, China; and [h]State Key Laboratory of Soil Erosion and Dryland Farming on the Loess Plateau, Institute of Soil and Water Conservation, Chinese Academy of Sciences & Ministry of Water Resources, 712100 Yangling, China

Contributed by Zhisheng An, May 29, 2020 (sent for review December 26, 2019; reviewed by Achim Bräuning and Hongyan Liu)

The Yellow River (YR) is the fifth-longest and the most sediment-laden river in the world. Frequent historical YR flooding events, however, have resulted in tremendous loss of life and property, whereas in recent decades YR runoff and sediment load have fallen sharply. To put these recent changes in a longer-term context, we reconstructed natural runoff for the middle reach of the YR back to 1492 CE using a network of 31 moisture-sensitive tree-ring width chronologies. Prior to anthropogenic interference that started in the 1960s, the lowest natural runoff over the past 500 y occurred during 1926 to 1932 CE, a drought period that can serve as a benchmark for future planning of YR water allocation. Since the late 1980s, the low observed YR runoff has exceeded the natural range of runoff variability, a consequence of the combination of decreasing precipitation and increasing water consumption by direct and indirect human activities, particularly agricultural irrigation. This reduced runoff has resulted in an estimated 58% reduction of the sediment load in the upper reach of the YR and 29% reduction in the middle reach.

tree rings | Yellow River | runoff reconstruction | sediment load | water consumption

The Yellow River (YR) is the cradle of Chinese civilization. Although the YR accounts for only 3% of China's water resources, it irrigates 13% of its cropland (1). Frequent historical "breach" (flow outside channel) and recent "cutoff" (low flow) events, mainly in the middle and lower YR basins, have resulted in considerable losses to lives and properties (2, 3). The upper-middle YR basins are densely populated and the main breadbasket of China, where agriculture, particularly in the irrigation districts of Ningxia and Inner Mongolia (Fig. 1), depends heavily on YR water resources. A multicentury-scale understanding of the factors influencing YR runoff is therefore crucial for effective water resource assessment and management, but the earliest observational record of YR runoff, beginning in 1919 CE at the Shanxian gauge station (*Materials and Methods*), is too short to study centennial-scale variability.

Since the start of the Anthropocene (4) in the 1960s, an increasing number of large-scale dams and reservoirs have been built in the main YR channel (5). In addition to this, water consumption by agricultural irrigation along the YR middle course has risen sharply (6). Human activities have ultimately and irreversibly changed YR natural characteristics (7, 8). Low-flow events have occurred frequently in recent decades, and there was even no water flow for several months each year in the lower YR course during 1995 to 1998 CE (9). Moreover, the sediment load of the YR has declined by ∼90% over the past 60 y (10), which significantly affects the ecosystems and the delta morphology of the YR estuary (11). As such, the amount of YR water consumed by human activities and the causes of sediment load reduction over these past few decades continue to be of great interest (12, 13).

Annually resolved tree-ring-based paleohydrological reconstructions reflect natural runoff variability, provide longer time series, and present a broader range of extremes than observational records (14, 15). Tree-ring data have therefore been used to reconstruct upper YR runoff variability over recent centuries (16, 17). Li et al. (18) also reconstructed middle YR runoff, but the tree-ring data used in that study are primarily derived from upper areas on and around the Tibetan Plateau and partly outside the YR basin (figure 1A in ref. 18), which may not necessarily capture runoff variability in the middle YR course well.

Significance

The Yellow River (YR) is the cradle of Chinese civilization. It supports agriculture, social prosperity, and human survival. YR runoff and sediment load have sharply fallen since the late 1980s. We reconstructed natural runoff history for the middle reach of the YR from 1492 to 2013 CE. We found that the recent low observed YR runoff is unprecedented over the past five centuries, mainly due to the combination of decreasing precipitation and increasing water consumption by human activities, particularly agricultural irrigation. Our results provide a valuable historical dataset for YR water management, as well as an important model for how to distinguish and quantify anthropogenic influence from natural variability in global change studies.

Author contributions: Y. Liu, H.S., and Z.A. designed research; Y. Liu, H.S., Z.A., C.S., Q.C., R.L., S.W.L., and Q.L. performed research; Y. Liu and H.S. contributed new reagents/analytic tools; Y. Liu, H.S., C.S., V.T., Q.C., R.L., S.W.L., Y.S., Q.L., C.F., W.Z., Y.Y., Z.J., Y.W., J.S., X.M., Y. Lei, L.W., X.L., M.R., L.C., and X.Z. analyzed data; and Y. Liu, H.S., Z.A., C.S., V.T., Q.C., and S.W.L. wrote the paper.

Reviewers: A.B., Friedrich Alexander University Erlangen-Nuremberg; and H.L., Peking University.

The authors declare no competing interest.

[1]To whom correspondence may be addressed. Email: liuyu@loess.llqg.ac.cn or anzs@loess.llqg.ac.cn.

This article contains supporting information online at https://www.pnas.org/lookup/suppl/doi:10.1073/pnas.1922349117/-/DCSupplemental.

First published July 20, 2020.

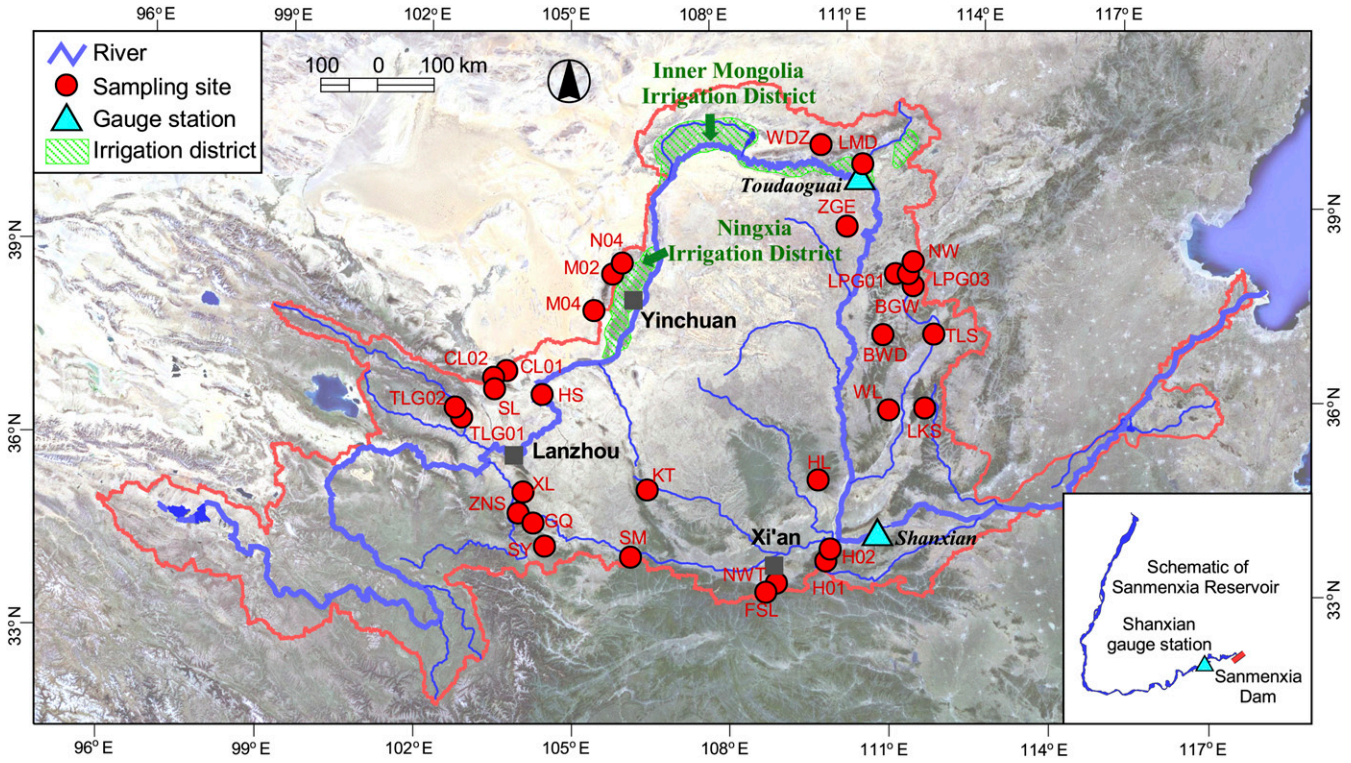

Fig. 1. Thirty-one tree-ring sites (red dots) in the middle-upper reaches of the YR. The thick blue line denotes the YR, and the thin blue line denotes the large tributaries along the river; blue triangles represent the gauge stations in the main channel, namely, Toudaoguai and Shanxian; the green shaded areas are irrigation districts. The map in the lower right corner shows the area of the Sanmenxia Reservoir.

Additionally, historical documents have been used to reconstruct YR runoff history (19, 20), but their interpretation is more subjective compared to tree-ring data. Our study, in contrast, is based on 31 moisture-sensitive tree-ring width chronologies collected within the upper-middle YR basins (Fig. 1 and *SI Appendix*, Table S1), which allowed us to reconstruct natural runoff for the middle YR course over the period 1492 to 2013 CE. Our reconstruction complements previous regional studies, and we also quantify the amount of anthropogenic YR water consumption in recent decades. Furthermore, our study calculates the reduction in YR sediment load caused by increasing human water consumption.

Results and Discussion

The first dam on the main YR channel was completed in 1961 CE in Sanmenxia, but the runoff at the Shanxian station prior to this date, from 1919 to 1960 CE, is considered largely unaltered by human activities (*Materials and Methods*). Over this period, the first principal component (PC1) of the 31 tree-ring chronologies (*Materials and Methods*) from the upper-middle YR basin strongly correlates with the Shanxian hydrological-year runoff (R_{87}; previous August to current July; $r = 0.76$; $P < 0.001$) (Fig. 2 *A* and *B*). This allowed us to reconstruct YR R_{87} back to 1492 CE (Fig. 2*C*) with robust statistical skill (*Materials and Methods* and *SI Appendix*, Table S2). Our reconstruction shares a common declining trend in recent decades with three other YR reconstructions from the source (16) to the middle reaches (19, 20) (*SI Appendix*, Fig. S1). Our reconstruction is in contrast to the reconstruction of Li et al. (18), who found a rising discharge trend for the middle reach of the YR since the late 1960s; however, their reconstruction used many tree-ring samples from far outside of the YR watershed.

Our reconstruction provides a record of natural YR runoff variability prior to large-scale human interference. Over the past 522 y, the average runoff of the YR is 410.24×10^8 m^3. Most of the extreme high/low runoff events (*Materials and Methods*) in the reconstruction prior to 1960 CE can be verified with historical documents (*SI Appendix*, Table S3). For example, the lowest YR flow since 1492 CE occurred during 1926 to 1932 CE, with a reconstructed average annual runoff of 297.53×10^8 m^3 (72.52% of overall average) and observed runoff of 308.87×10^8 m^3 (75.29% of overall average). Documents show that in the summer of 1928 CE, flow in the main YR tributaries, such as the Jinghe and Weihe Rivers, was completely cut off, and horses and chariots could traverse dry riverbeds (21). This flow level could be a benchmark for future judicious planning of water allocation. The Fenghe and Weihe Rivers, the main branches of the YR, were also depleted in 1691 CE as documented (*SI Appendix*, Table S3).

Our reconstruction also allows us to model theoretical YR runoff, without human interference, for the more recent period from 1960 CE forward and thus to assess the recent effects of human activities. We found that both observed and reconstructed runoff declined after the late 1930s, but the divergence between them has been increasing (Fig. 2*C*). Particularly, since the late 1980s, observed runoff has fallen out of its natural range of variability. We hypothesize that this runoff decline in recent decades can be explained by two factors.

First, runoff in the middle course of the YR closely relies on regional precipitation (22), which is determined by the strength of the Asian summer monsoon (ASM). Our YR runoff reconstruction is strongly correlated ($r = 0.86$, 1566 to 2013 CE, $P < 0.001$; *SI Appendix*, Fig. S2) with an ASM precipitation reconstruction from the western Loess Plateau (34°–41°N, 100°–107°E; ref. 23). It should be noted that all 10 tree-ring chronologies used for the precipitation reconstruction are also part of our YR runoff reconstruction and that the reconstructions are therefore not independent (*Materials and Methods* and *SI Appendix*, Table S1).

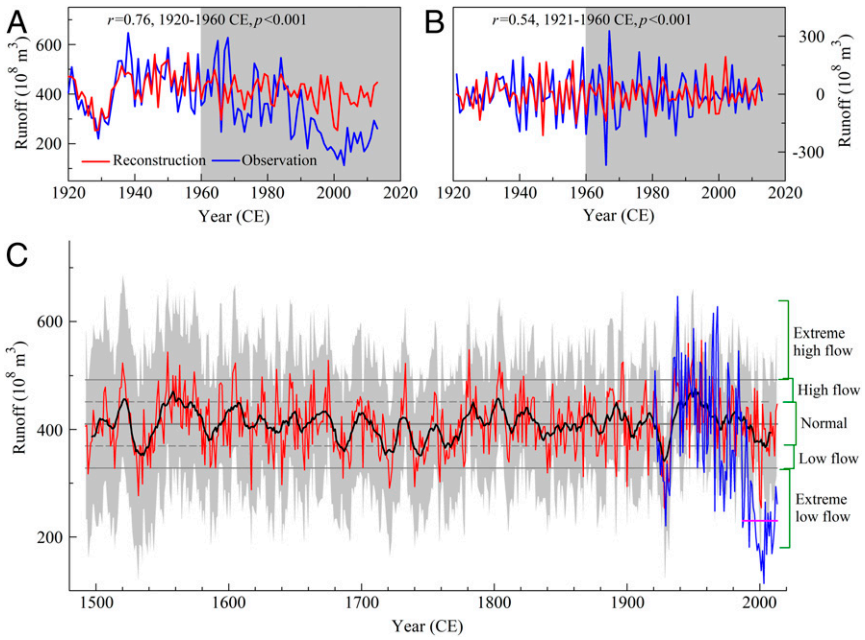

Fig. 2. Hydrological year (previous August to current July) runoff reconstruction at the Shanxian gauge station of the YR. Comparison between the observed (blue) and the reconstructed (red) runoff (*A*). Comparison of the first difference of *A* (*B*). Runoff reconstruction (red) from 1492 to 2013 CE based on the calibration period 1920 to 1960 CE, which preceded construction of the Sanmenxia Dam (*C*). The black curve is the 11-y moving average of the reconstruction. The blue curve superimposed on the reconstruction denotes the observed annual runoff from 1920 to 2013 CE. The shaded area represents the ±2 SE bars. The short pink horizontal line (lower right) represents the average observed runoff from 1987 to 2013 CE. The solid gray horizontal lines indicate the mean value of the reconstruction, and the boundaries for extremely high/low runoff, respectively. The dashed gray horizontal lines indicate the boundaries for high/low runoff, respectively (*Materials and Methods*).

Over the past 80 y, ASM precipitation has shown a decreasing trend (23), so the amount of water recharge in the branch rivers of the upper-middle YR course has been largely declining (the oblique line in *SI Appendix*, Fig. S2). There are no other regional precipitation reconstructions with annual resolution beyond our dataset in the YR basin. Therefore, we employ the Climatic Research Unit (CRU) (24) and Global Precipitation Climatology Centre (GPCC) (25) precipitation on the Loess Plateau region (33.5–40.5°N; 100–111°E) as two additional independent series to represent regional precipitation variability. Both CRU and GPCC precipitation (from previous August to current July) are significantly positively correlated ($r = 0.72$ and $r = 0.73$, $P < 0.001$; 1937 to 2013 CE) with the YR runoff reconstruction (*SI Appendix*, Fig. S3). This result further confirms the relationship between runoff and regional precipitation. In addition, periodicity analysis (*Materials and Methods*) shows that both the Asian monsoon precipitation (23) and YR runoff are influenced by atmospheric circulation systems, such as the El Niño–Southern Oscillation (ENSO) and

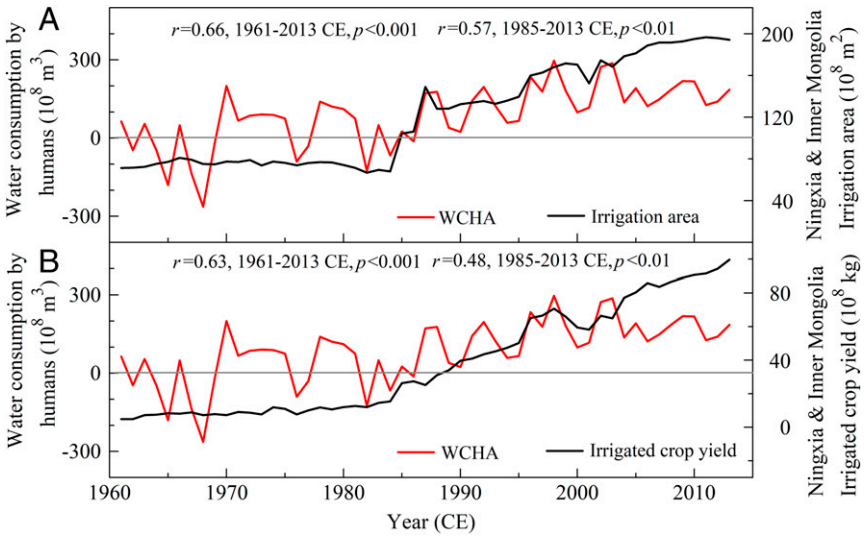

Fig. 3. Relationship between the WCHA and agriculture in the irrigation districts of Ningxia and Inner Mongolia during 1961 to 2013 CE. Irrigation area (*A*) and Irrigated crop yield (*B*).

Pacific Decadal Oscillation (PDO). We also found that the association between observed runoff and regional precipitation series, that is, reconstructed precipitation, CRU precipitation, and GPCC precipitation (*SI Appendix*, Fig. S4), has been decreasing in recent years, which likely results from the intensification of human activities.

Second, anthropogenic water consumption directly reduced YR runoff in an unprecedented and irreversible way after the Sanmenxia Dam was built in 1961 CE. By subtracting the observed runoff (1961 to 2013 CE) from the reconstructed natural runoff, we obtained a time series of the year-to-year variability in water consumption by human activities (WCHA, the red line in Fig. 3). We found that WCHA has increased dramatically since 1961 CE, and even further after more dams came into operation in 1986 CE. It should be noted that tree-ring width is very sensitive to dry years but less responsive to heavy rainfall events because if the plant's demand for water is exceeded growth will respond no further (26). Therefore, our reconstruction is less skillful to capture natural runoff of years with excessive precipitation (and runoff) (*SI Appendix*, Fig. S5). Since the WCHA was calculated by subtracting the observed from the modeled runoff, this computation becomes sensitive to years when the reconstructed runoff underestimates the true runoff. Therefore, WCHA values were negative in some years (Fig. 3). If WCHA had not escalated, our reconstruction model suggests that the theoretical average runoff (1987 to 2013 CE) would have been 390.88×10^8 m^3, almost double the actual observed runoff over the same period (230.21×10^8 m^3). Furthermore, theoretically, there should have been two high-flow years over this period (2/27 = 7.41%), but instead there were 25 extreme low-flow years (92.6%) and no high-flow years at all in the observed record (Fig. 4).

As we calculated that 64% of the total water consumption by agricultural irrigation in the most recent two decades (1998 to 2017 CE) was consumed by the Ningxia and Inner Mongolia irrigation regions (NIMI) (*Materials and Methods*). Meanwhile, crop yields and acreage in NIMI were strongly positively correlated with WCHA (Fig. 3 and *SI Appendix*, Fig. S6), suggesting that agricultural irrigation in these two regions played a vital role in the curtailment of YR runoff (27, 28). Agriculture consumes most of the YR's water, but with relatively low productivity. As natural precipitation supply declines and demand for water increases, water allocation policy should be carefully designed to balance needs of agriculture, industry, and ecosystems. At the same time, improvement of water-use efficiency in agriculture and industry should benefit from technological advances. In addition to agricultural irrigation, human afforestation also had impact on water consumption. Revegetation increases evapotranspiration, which can cause a decrease in runoff. The explanation ratio (R square) of the relationship between revegetation (indicated by revegetated area and leaf area index change) and runoff decrease on the Loess Plateau was 31% (29). This indicates that human afforestation was another important nonclimatic factor influencing water consumption in recent decades. Ultimately, in addition to climate, the reduction in the runoff of the YR is mainly due to various human activities, such as direct (e.g., water withdrawal for irrigation, etc.) and indirect (e.g., revegetation/afforestation) human activities.

Another aspect of YR variability influenced by recent anthropogenic activities is sediment load. The YR once carried the largest sediment load in the world (6), but in recent decades that load has decreased dramatically (10). Sediment reduction can actually improve the water quality of the YR and also effectively prevent aggradation of the channel bed downstream. However, excessive reduction of sediment load will threaten the stability and persistence of the delta downstream. Therefore, the causes of the sharp reduction of the sediment load of YR have become the focus of researchers and policy makers.

We found that WCHA was strongly negatively correlated with sediment load at Toudaoguai ($r = -0.76$; $P < 0.01$; 1961 to 2013 CE) and Shanxian station ($r = -0.54$; $P < 0.01$; 1961 to 2013 CE) (Fig. 5), indicating that WCHA for agricultural irrigation in NIMI was the primary anthropogenic factor causing reduced YR sediment load since the 1960s. That is to say, 58% of the reduction of sediment load in Toudaoguai (upper reach) and 29% in Shanxian (middle reach) was associated with WCHA. The decreasing runoff and water volume in YR weakened hydrodynamic forces and thereby attenuated the capacity of sediment transportation and enhanced sediment deposition (9). These factors reduced sediment load and clarified the water in the YR main channel (30). In addition, government-sponsored measures, such as construction of tens of thousands of check dams, soil and water conservation, and afforestation on the Loess Plateau, which is the largest sediment source of YR, also contributed about 30% to the

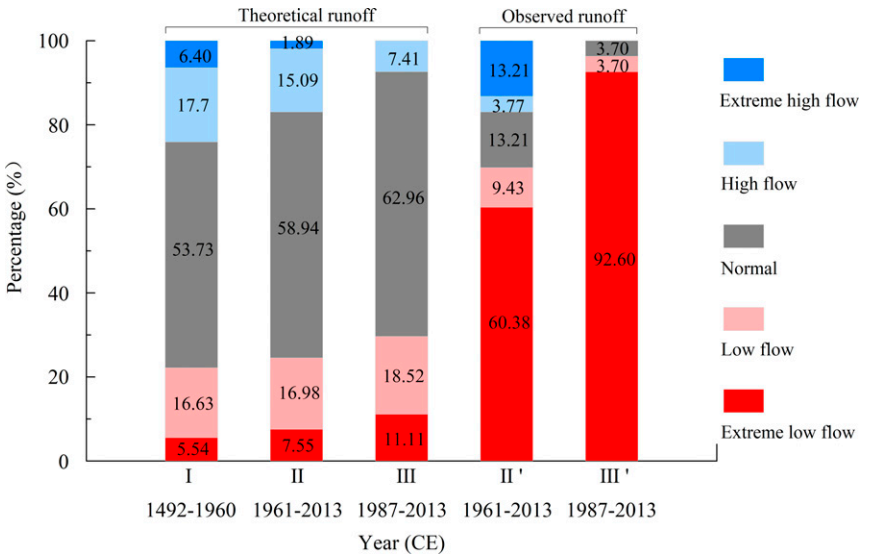

Fig. 4. Percentage of extremely high/extremely low, high/low, and normal years in the theoretical observed runoff during three periods: 1492 to 1960 CE (I), 1961 to 2013 CE (II and II′), and 1987 to 2013 CE (III and III′).

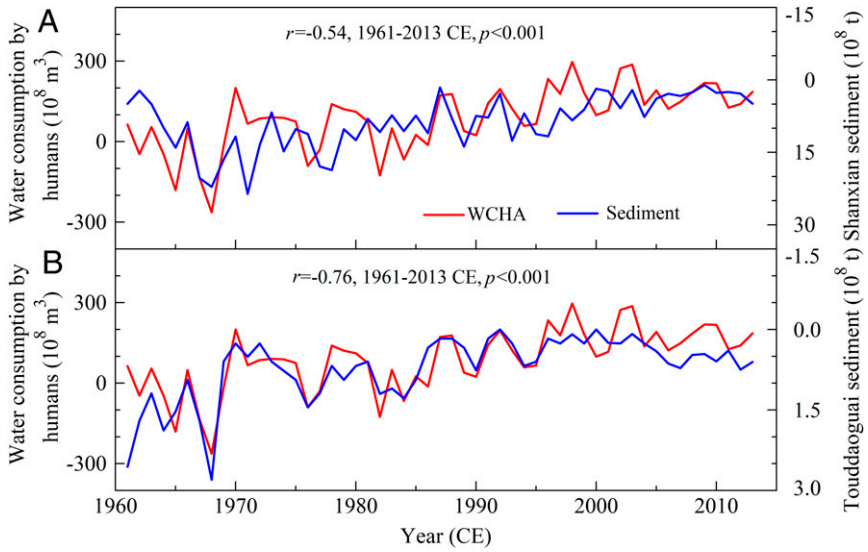

Fig. 5. Relationship between WCHA and sediment load from two stations on the YR (1961 to 2013 CE): the Shanxian station (*A*) and the Toudaoguai station (*B*).

reduction of the YR sediment load (6). Check dams can efficiently block the sediments in gullies, and the increasing vegetation coverage can reduce soil erosion (6, 11, 31). All these measures have thus prevented sediment transport into the YR (22).

Conclusions. Our study puts the recent runoff records of YR into a long-term context to assess the effects of human activities. We found that the curtailed runoff of the YR since the late 1980s was unprecedented over the past 522 y. Human activities, mainly expansive agricultural irrigation in the upper course, have contributed to reduced runoff and sediment load in the upper-middle course of the YR. If these human activities continue to intensify, future YR runoff will be further reduced, and this will negatively impact agriculture, human lives, and socioeconomic development in the middle and lower basins of the YR. To reduce the risk of recurring cutoff of streamflow in the YR lower basin, water should be allocated judiciously. Cautious policy can balance water allocation among the needs of agriculture, industry, and ecosystems. From this point of view, our reconstructed YR natural runoff series are important for future YR water resource management. In addition, our study exhibits an example of how to distinguish and quantify anthropogenic influence from natural variability in global change studies.

Materials and Methods

Data. Observed runoff and sediment load data (1919 to 2013 CE) from the Shanxian (34°49′N, 111°09′E) and Toudaoguai (40°16′N, 111°04′E) gauging stations were obtained from the Bureau of Hydrology, Yellow River Conservancy Commission. Sanmenxia Dam was completed in April 1961 CE; therefore, river discharge after 1961 CE is not considered natural. Water consumption data for 1998 to 2017 CE were obtained from Yellow River Water Resources Bulletin (www.yrcc.gov.cn/; all data and website information are available from the authors upon request). The irrigation area and crop yields data were collected from the Statistical Yearbook of Ningxia and Inner Mongolia.

Basic Theory of Tree-Ring Runoff Reconstruction. In principle, precipitation in river basins affects both tree growth and runoff supply. Therefore, moisture-sensitive tree rings are a powerful tool that can be used to directly reconstruct precipitation and to indirectly reconstruct runoff changes (32–41). Such reconstructions contribute important data to water resource allocation and management. There are important preconditions for applying dendrochronology to reconstruct runoff in historical periods; for example, rivers must have no big dams and must be without prominent human disturbance such as the large-scale withdrawal of irrigation water (38).

Nested Principal Component Reconstruction Method. Our tree-ring network consists of 31 moisture-sensitive tree-ring width chronologies from the upper-middle reaches of the YR, comprising in total 1,707 tree-ring cores (Fig. 1 and *SI Appendix*, Table S1). Among them, 21 chronologies have already been published (42–58), 6 chronologies were previously published but have been updated (47, 59–63), and 4 chronologies represent unpublished data (*SI Appendix*, Table S1).

The lengths of the 31 tree-ring chronologies that constitute the network are not uniform. When we apply traditional principal component reconstruction based on such a matrix, the length of the resulting reconstruction time series is greatly shortened. To maximize the length of YR runoff reconstruction, we use a nested principal component analysis (PCA) method to extract PCs from the tree-ring chronologies (64, 65). First, we permute the chronologies to a step-like matrix with long chronologies on the left and short chronologies on the right. Then, we perform PCA to extract PCs step by step. For each step, we use all of the available chronologies. By designing linear regression models, we use the PC1 series as an independent variable to enable reconstruction at its highest explanatory variance. The split calibration–verification method (66, 67) is adopted to test the stability of the regression models over the common period (1920 to 1960 CE) of the observed runoff and the PC1 series. Consequently, we get *N* series of reconstructed runoff where *N* equals to the number of steps. We also arrange reconstructions in a step-like matrix named the reconstructed matrix, which has a flat top or bottom. Meanwhile, the statistical parameters for the verification period, including R^2, *SE*, *RE* (reduction of error), *CE* (coefficient of efficiency), and *ST* (sign test) for each reconstruction are also obtained. Generally, *RE* and *CE* values greater than zero indicate a rigorous model skill. Larger values of *RE* and *CE* indicate better results. Moreover, the values of *CE* are more rigorous and are typically lower than those of *RE* (*SI Appendix*, Table S2).

Because inhomogeneity generally occurs both in the upper and lower parts of the tree-ring time matrix, such procedures of the PC reconstruction are conducted separately for the lower and upper triangular step-like matrix. Thus, the column number of the reconstructed matrix *N* equals the sum of number of steps in the lower and upper triangular matrix minus 1. There must be one shortest reconstructed series (marked as $X_{ishortest}$) in the reconstructed matrix, which is reconstructed by the largest number of chronologies. Eventually, we merge the reconstructed matrix into one series. Except for the $X_{ishortest}$ series, which we adopt entirely, we only use the segment from the start (end) of one step to the start (end) of the next step for the reconstructed matrix of the lower (upper) triangular part, so that the statistical parameters of these reconstructed series are also merged into series according to the corresponding time interval. Due to the differences of mean value and variance among the reconstructed series, we normalize

them before the merging procedure. Here we establish the $X_{ishortest}$ base according to the formula

$$Y_i = \frac{X_i + a_i}{b_i}, i = 1, \ldots N, i \neq \text{ishortest}.$$

$$b_i = \sqrt{D(X_i)/D(X_{ishortest})}, a_i = b_i * E(X_{ishortest}) - E(X_i).$$

X and Y are reconstructed series before and after the unification; E and D denote calculating the average and variance.

The uncertainty (SE) of the reconstruction was estimated according to the formula

$$\text{SE} = \sqrt{\frac{1}{n-2}\sum_{i=1}^{n}(\hat{y}_i - y_i)^2},$$

where $\hat{y}_i$ and y_i denote the reconstructed and observed runoff, respectively, and n is the length of the reconstructed series.

Definition of High/Low Stream Flow Years in This Paper. According to the Chinese hydrological forecasting standard (68), we defined extreme high/low flow years based on the relationship between runoff value of each year and the value of the multiyear average (410.24×10^8 m^3, 1492 to 2013 CE). An extreme high-flow year is one with runoff 20% (runoff $>492.30 \times 10^8$ m^3) greater than average; a high-flow year is one with runoff 10% (runoff $>451.27 \times 10^8$ m^3) greater than average; a normal year is one with runoff within 10% (369.22×10^8 m^3 $\leq$ runoff $\leq$ 451.27×10^8 m^3) of the average; a low-flow year is one with runoff 10% (runoff $<369.22 \times 10^8$ m^3) below average; and an extreme low-flow year is one with runoff 20% (runoff $<328.20 \times 10^8$ m^3) below average. During 1492 to 1960 CE (469 y), there were 30 (30/469 = 6.4%)/26 (5.5%) extreme high/low flow years and 83 (17.7%)/78 (16.6%) high/low flow years (Fig. 4). During 1961 to 2013 CE (53 y), there should be 1 (1.9%)/4 (7.6%) extreme high/low flow years and 8 (15.1%)/9 (17.0%) high/low flow years in the reconstructed theoretical runoff. However, during the same period 1961 to 2013 CE, the observed runoff showed that there were 7 (13.2%)/32 (60.4%) extreme high/low flow years and 2 (3.8%)/5 (9.4%) high/low flow years.

Periodicity Analysis of the YR Runoff Reconstruction. We calculated the periodicities in YR runoff reconstruction using the multitaper method of spectral analysis (69), which is a powerful tool in spectral estimation. The result shows that the YR runoff displays 2.1 to 3.5a, 10.0a, and 24.4a cycles at 95% confidence level and 6.4a, 8.3a, 13.0a, 48.8a, and 204a cycles at 90% confidence level (*SI Appendix*, Fig. S7). The interannual and decadal cycles are related to the frequency domains of ENSO and PDO, respectively (70).

Water Consumption for Agricultural Irrigation. The main WCHA is agricultural irrigation in Inner Mongolia, Ningxia, Gansu, Shanxi, and Shaanxi provinces along the YR, with an average total amount of 130.44×10^8 m^3/y over the observation period 1998 to 2017 CE. Water withdrawal for other types of usage is 52.75×10^8 m^3/y (Yellow River Water Resources Bulletin of 1998 to 2017 CE). From 1998 to 2017 CE, the average water consumption for irrigation in Ningxia and Inner Mongolia provinces was 30.98×10^8 m^3/y (23.75% of the five provinces) and 52.42×10^8 m^3/y (40.19% of the five provinces), respectively. This indicates that Ningxia and Inner Mongolia were the main irrigation areas within the YR basin.

Data and Materials Availability. All data are available in the paper or *SI Appendix*.

ACKNOWLEDGMENTS. This work was supported by the Chinese Academy of Sciences (CAS) (QYZDJ–SSW–DQC021), National Natural Science Foundation of China (41630531), CAS grants (XDB40010300, XDA23070202, GJHZ1777, DQGG0104, and 2016361), and grants from the Institute of Earth Environment, Chinese Academy of Sciences, and the State Key Laboratory of Loess and Quaternary Geology. This is the contribution of the Sino-Swedish Tree-Ring Research Center (no. 201901).

1. D. Ren, X. Xu, Y. Hao, G. Huang, Modeling and assessing field irrigation water use in a canal system of Hetao, upper Yellow River basin: Application to maize, sunflower and watermelon. *J. Hydrol.* **532**, 122–139 (2016).
2. T. S. Bianchi, M. A. Allison, Large-river delta-front estuaries as natural "recorders" of global environmental change. *Proc. Natl. Acad. Sci. U.S.A.* **106**, 8085–8092 (2009).
3. Y. Chen, J. P. M. Syvitski, S. Gao, I. Overeem, A. J. Kettner, Socio-economic impacts on flooding: A 4000-year history of the Yellow River, China. *Ambio* **41**, 682–698 (2012).
4. S. L. Lewis, M. A. Maslin, Defining the anthropocene. *Nature* **519**, 171–180 (2015).
5. Y. Yu *et al.*, Effects of dams on water and sediment delivery to the sea by the Huanghe (Yellow River): The special role of water-sediment modulation. *Anthropocene* **3**, 72–82 (2013).
6. S. Wang *et al.*, Reduced sediment transport in the Yellow River due to anthropogenic changes. *Nat. Geosci.* **9**, 38–41 (2016).
7. T. Yang *et al.*, A spatial assessment of hydrologic alteration caused by dam construction in the middle and lower Yellow River, China. *Hydrol. Processes* **22**, 3829–3843 (2008).
8. T. Zhao, K. S. Richards, H. Xu, H. Meng, Interactions between dam-regulated river flow and riparian groundwater: A case study from the Yellow River, China. *Hydrol. Processes* **26**, 1552–1560 (2012).
9. M. Giordano *et al.*, "Water management in the Yellow River basin: Background, current critical issues and future research needs" (Comprehensive Assessment Research Report 3, Comprehensive Assessment Secretariat, Colombo, Sri Lanka, 2004).
10. Y. Yu *et al.*, New discharge regime of the Huanghe (Yellow River): Causes and implications. *Cont. Shelf Res.* **69**, 62–72 (2013).
11. H. Wang *et al.*, Recent changes in sediment delivery by the Huanghe (Yellow River) to the sea: Causes and environmental implications in its estuary. *J. Hydrol.* **391**, 302–313 (2010).
12. X. Mu, W. Wang, P. Gao, G. Zhao, Progress and discussion on sediment load variation research of the Yellow River. *Yellow River* **36**, 1–7 (2014).
13. G. Zhao *et al.*, Quantifying the impact of climate variability and human activities on streamflow in the middle reaches of the Yellow River basin, China. *J. Hydrol.* **519**, 387–398 (2014).
14. D. J. Sauchyn, J. M. St-Jacques, B. H. Luckman, Long-term reliability of the Athabasca River (Alberta, Canada) as the water source for oil sands mining. *Proc. Natl. Acad. Sci. U.S.A.* **112**, 12621–12626 (2015).
15. C. A. Woodhouse, J. J. Lukas, Multi-century tree-ring reconstructions of Colorado streamflow for water resource planning. *Clim. Change* **78**, 293–315 (2006).
16. X. Gou *et al.*, Streamflow variations of the Yellow River over the past 593 years in western China reconstructed from tree rings. *Water Resour. Res.* **43**, 1820–1830 (2007).
17. X. Gou *et al.*, Tree ring based streamflow reconstruction for the Upper Yellow River over the past 1234 years. *Chin. Sci. Bull.* **55**, 4179–4186 (2010).
18. J. Li *et al.*, Deciphering human contributions to Yellow River flow reductions and downstream drying using centuries-long tree ring records. *Geophys. Res. Lett.* **46**, 898–905 (2019).
19. W. Pan, J. Zheng, L. Xiao, F. Yan, The relationship of nature runoff changes in flood-season of middle Yellow River and Yongding River, 1766–2004. *Acta Geogr. Sin.* **68**, 975–982 (2013).
20. G. Wang *et al.*, Natural annual runoff estimation from 1470 to 1918 for Sanmenxia gauge station of Yellow River. *Adv Water Sci* **10**, 170–176 (1999).
21. A. Dong, J. Wang, Y. Li, The disaster situation and reasons for the severe drought event of 1928 in Yellow River valley. *Ganhanqu Ziyuan Yu Huanjing* **28**, 151–157 (2014).
22. J. Best, Anthropogenic stresses on the world's big rivers. *Nat. Geosci.* **12**, 7–21 (2019).
23. Y. Liu *et al.*, Anthropogenic aerosols cause recent pronounced weakening of Asian summer monsoon relative to last four centuries. *Geophys. Res. Lett.* **46**, 5469–5479 (2019).
24. I. Harris, P. D. Jones, T. J. Osborn, D. H. Lister, Updated high-resolution grids of monthly climatic observations–the CRU TS3.10 dataset. *Int. J. Climatol.* **34**, 623–642 (2014).
25. U. Schneider *et al.*, GPCC's new land surface precipitation climatology based on quality-controlled in situ data and its role in quantifying the global water cycle. *Theor. Appl. Climatol.* **115**, 15–40 (2014).
26. H. C. Fritts, Ed., *Tree Rings and Climate*, (Academic Press, London, 1976).
27. R. Q. Grafton *et al.*, Global insights into water resources, climate change and governance. *Nat. Clim. Chang.* **3**, 315–321 (2013).
28. S. Piao *et al.*, The impacts of climate change on water resources and agriculture in China. *Nature* **467**, 43–51 (2010).
29. X. Feng *et al.*, Revegetation in China's Loess Plateau is approaching sustainable water resource limits. *Nat. Clim. Chang.* **6**, 1019–1022 (2016).
30. H. Wang *et al.*, Stepwise decreases of the Huanghe (Yellow River) sediment load (1950–2005): Impacts of climate change and human activities. *Global Planet. Change* **57**, 331–354 (2007).
31. Y. Chen *et al.*, Balancing green and grain trade. *Nat. Geosci.* **8**, 739–741 (2015).
32. U. Akkemik, R. D'Arrigo, P. Cherubini, N. Kose, G. C. Jacoby, Tree-ring reconstructions of precipitation and streamflow for north-western Turkey. *Int. J. Climatol.* **28**, 173–183 (2008).
33. F. Chen, Y. Yuan, S. Yu, Tree-ring indicators of rainfall and streamflow for the Ili-Balkhash basin, Central Asia since CE 1560. *Palaeogeogr Palaeocl* **482**, 48–56 (2017).
34. N. Devineni, U. Lall, N. Pederson, E. Cook, A tree-ring-based reconstruction of Delaware River basin streamflow using hierarchical Bayesian regression. *J. Clim.* **26**, 4357–4374 (2013).
35. A. Lara *et al.*, Reconstructing streamflow variation of the Baker River from tree-rings in Northern Patagonia since 1765. *J. Hydrol.* **529**, 511–523 (2015).
36. Y. Liu *et al.*, Tree-ring hydrologic reconstructions for the Heihe River watershed, western China since AD 1430. *Water Res.* **44**, 2781–2792 (2010).
37. E. R. Lutz, A. F. Hamlet, J. S. Littell, Paleoreconstruction of cool season precipitation and warm season streamflow in the Pacific Northwest with applications to climate change assessments. *Water Resour. Res.* **48**, 182–205 (2012).

38. R. S. Maxwell, A. E. Hessl, E. Cook, N. Pederson, A multispecies tree ring reconstruction of Potomac River streamflow (950–2001). *Water Resour. Res.* **47**, 159–164 (2011).
39. J. Patskoski, A. Sankarasubramanian, H. Wang, Reconstructed streamflow using SST and tree-ring chronologies over the southeastern United States. *J. Hydrol.* **527**, 761–775 (2015).
40. S. K. Shah, A. Bhattacharyya, V. Chaudhary, Streamflow reconstruction of Eastern Himalaya River, Lachen "Chhu", North Sikkim, based on tree-ring data of Larix griffithiana from Zemu glacier basin. *Dendrochronologia* **32**, 97–106 (2014).
41. B. Yang, X. Chen, Y. He, J. Wang, C. Lai, Reconstruction of annual runoff since CE 1557 using tree-ring chronologies in the upper Lancang-Mekong River basin. *J. Hydrol.* **569**, 771–781 (2019).
42. Q. Cai, Y. Liu, The development of a tree-ring width chronology and the May–June mean temperature variability in Wulu Mountain, Shanxi province of north-central China. *Quatern Sci* **33**, 511–517 (2013).
43. Q. Cai, Y. Liu, Y. Lei, G. Bao, B. Sun, Reconstruction of the March–August PDSI since 1703 AD based on tree rings of Chinese pine (*Pinus tabulaeformis* Carr.) in the Lingkong mountain, southeast Chinese Loess Plateau. *Clim. Past* **10**, 509–521 (2014).
44. Q. Cai, Y. Liu, H. Song, J. Sun, Tree-ring-based reconstruction of the April to September mean temperature since 1826 AD for north-central Shaanxi province, China. *Sci. China. Ser. D Earth Sci.* **51**, 1099–1106 (2008).
45. M. Hughes, X. Wu, X. Shao, G. Garfin, A preliminary reconstruction of rainfall in northcentral China since AD 1600 from tree-ring density and width. *Quat. Res.* **42**, 88–99 (1994).
46. Q. Li *et al*., Reconstruction of annual precipitation since 1686 A.D. from Ningwu region, Shanxi Province. *Quat. Sci.* **26**, 999–1006 (2006).
47. Y. Liu *et al*., Seasonal precipitation in the south-central Helan Mountain region, China, reconstructed from tree-ring width for the past 224 years. *Can. J. For. Res.* **35**, 2403–2412 (2005).
48. Y. Liu, Y. Lei, B. Sun, H. Song, Q. Li, Annual precipitation variability inferred from tree-ring width chronologies in the Changling-Shoulu region, China, during AD 1853-2007. *Dendrochronologia* **31**, 290–296 (2013).
49. Y. Liu, Y. Lei, B. Sun, H. Song, J. Sun, Annual precipitation in Liancheng, China, since 1777 AD derived from tree rings of Chinese pine (*Pinus tabulaeformis* Carr.). *Int. J. Biometeorol.* **57**, 927–934 (2013).
50. Y. Liu *et al*., Temperature variations recorded in *Pinus tabulaeformis* tree rings from the southern and northern slopes of the central Qinling Mountains, central China. *Boreas* **38**, 285–291 (2009).
51. Y. Liu, N. Liu, H. Song, G. Bao, W. Wang, Reconstructed mean air temperature from January to July at the divide sampling site in the Mid-Qinling mountains with tree-ting widths. *Adv. Clim. Chang. Res.* **5**, 260–265 (2009).
52. Y. Liu *et al*., Tree-ring width based May–June mean temperature reconstruction for Hua mountains since AD 1558 and 20th century warming. *Quat. Sci.* **29**, 1–8 (2009).
53. Y. Liu *et al*., Tree-ring-width-based PDSI reconstruction for central Inner Mongolia, China over the past 333 years. *Clim. Dyn.* **48**, 867–879 (2017).
54. H. Song, Y. Liu, Q. Li, H. Linderholm, Tree-ring derived temperature records in the central Loess Plateau, China. *Quat. Int.* **283**, 30–35 (2013).
55. H. Song *et al*., The climatic response of *Pinus tabulaeformis* Carr. in Mt. Zhuni, Gansu. *J Earth Environ* **8**, 119–126 (2017).
56. C. Sun *et al*., Tree-ring-based precipitation reconstruction in the source region of Weihe River, northwest China since AD 1810. *Int. J. Climatol.* **38**, 3421–3431 (2018).
57. J. Sun, Y. Liu, Y. Wang, G. Bao, B. Sun, Tree-ring based runoff reconstruction of the upper Fenhe River Basin, North China, since 1799 AD. *Quat. Int.* **283**, 117–124 (2013).
58. X. Zhang *et al*., Interannual variability of PDSI from tree-ring widths for the past 278 years in Baotou, China. *Trees (Berl.)* **31**, 1531–1541 (2017).
59. Q. Cai, Y. Liu, G. Bao, Y. Lei, B. Sun, Tree-ring-based May–July mean temperature history for Lüliang Mountains, China, since 1836. *Chin. Sci. Bull.* **55**, 3008–3014 (2010).
60. Y. Liu *et al*., Reconstruction of may–july precipitation in the north Helan mountain, Inner Mongolia since AD 1726 from tree-ring late-wood widths. *Chin. Sci. Bull.* **49**, 405–409 (2004).
61. Y. Liu, B. Sun, H. Song, Y. Lei, C. Wang, Tree-ring-based precipitation reconstruction for Mt. Xinglong, China, since AD 1679. *Quat. Int.* **283**, 46–54 (2013).
62. Y. Ma *et al*., A standardized precipitation evapotranspiration index reconstruction in the Taihe Mountains ysing tree-ring widths for the last 283 years. *PLoS One* **10**, e0133605 (2015).
63. H. Song, Y. Liu, PDSI variations at Kongtong Mountain, China, inferred from a 283-year *Pinus tabulaeformis* ring width chronology. *J. Geophys. Res. Atmos.* **116**, D22111 (2011).
64. E. Cook, R. D'Arrigo, M. Mann, A well-verified, multiproxy reconstruction of the winter North Atlantic Oscillation Index since A.D. 1400. *J. Clim.* **15**, 1754–1764 (2001).
65. D. Meko, Dendroclimatic reconstruction with time varying predictor subsets of tree indices. *J. Clim.* **10**, 687–696 (1997).
66. E. Cook, D. M. Meko, D. W. Stahle, M. K. Cleaveland, Drought reconstructions for the continental United States. *J. Clim.* **12**, 1145–1162 (1999).
67. H. C. Fritts, Ed., *Reconstructing Large-Scale Climatic Patterns from Tree-Ring Data*, (The University of Arizona Press, Tucson, AZ, 1991).
68. Hydrology Bureau of Ministry of Water Resources of China, *Standard for Hydrological Information and Hydrological Forecasting (GB/T 22482–2008)*, (China Standard Press, Beijing, 2008).
69. M. E. Mann, J. M. Lees, Robust estimation of background noise and signal detection in climatic time series. *Clim. Change* **33**, 409–445 (1996).
70. K. A. Tamaddun, A. Kalra, M. Bernardez, S. Ahmad, Multi-scale correlation between the western US snow water equivalent and ENSO/PDO using wavelet analyses. *Water Resour. Res.* **31**, 2745–2759 (2017).